



The spatial properties and local active control of road noise

Stephen J. Elliott, Woomin Jung and Jordan Cheer

Institute of Sound and Vibration Research, University of Southampton, SO17 1BJ, UK

Summary

The spatial performance of local active control systems depends on the correlation properties of the primary sound field. Previously this sound field has generally been assumed to be diffuse when simulating active control performance. In this study the spatial properties of the primary sound field due to road noise in a car were measured using the spectral density matrix calculated from the outputs of an array of 25 microphones in front of a headrest, into which a number of secondary sources had been integrated. The spatial correlation properties of the primary field were estimated and inverse methods were also used to estimate the sources of the road noise. Predictions were then made of the performance of local active sound controllers using the secondary sources in the headrest.

PACS no. 43.50.Ki, 43.50.Lj

1. Introduction

Road noise in cars is generated by the interaction between the tyres and the road surface and its transmission into the cabin is mainly structure-borne at low frequencies [1,2]. It can be a dominant source of noise at higher speeds and various systems have been used to control it passively or actively [1,2,3]. Previous active noise control systems for road noise have typically used accelerometers on the suspension and body to derive reference signals and the car's audio loudspeakers as secondary sources [3]. The acoustics of the typical car interior limit the frequency of operation of such systems to about 200 Hz [4]. There is considerable interest in controlling road noise at higher frequencies using more local active control systems, with loudspeakers located in the headrests for example [5,6].

The performance of such a local control system depends on the local geometry of the head and headrest [7], but also on the spatial properties of the primary sound field [8]. This paper is concerned with understanding these spatial properties and their effect on local active control systems. A general formulation is presented that allows the performance of such a local control system to be predicted from the calculated and measured properties of the sound field. After discussing some

illustrative results for idealized primary fields, some experiments are described in a car, in which the spatial properties of the road noise were measured at an array of microphones. This data is then used to predict the levels of active control that can be achieved with two loudspeakers in the headrest.

2. General theory and free field simulations

An illustration of the physical arrangement assumed here is shown in Fig. 1(a). An array of primary sources, of source strengths $\mathbf{v}^T = [v_1, v_2 \dots v_{Nv_2}]$, is assumed to generate the spatially random pressure field under control. This field is detected by a set of reference sensors producing signals $\mathbf{x}^T = [x_1, x_2 \dots x_{Nx}]$, which are used to drive a set of secondary sources with signals $\mathbf{u}^T = [u_1, u_2 \dots u_{Nu}]$. The region of control is assumed to be monitored by a set of sensors with outputs $\mathbf{y}^T = [y_1, y_2 \dots y_{Ny}]$, some of which are used to define the cost function used in the design of the control system. In the formulation used here, all the signals are assumed to be at a single frequency and proportional to $e^{j\omega t}$, although this dependence on ω is suppressed for notational convenience. The

signals are, however, assumed to be random variables, with their average properties defined by spectral density matrices, as described, for example, in [5]. The spectral density matrix defining the primary source strengths, for example, is given by

$$\mathbf{S}_{vv} = E[\mathbf{v}^H \mathbf{v}], \quad (1)$$

where the superscript H denotes the Hermitian, complex conjugate, transpose and E denotes the expectation operator. The diagonal elements of \mathbf{S}_{vv} are the power spectral densities of each individual primary source, and the off-diagonal terms are the cross spectral densities between these sources.

The block diagram for the system is illustrated in Fig. 1(b), where the primary sources, \mathbf{v} , generate the reference signals, \mathbf{x} , and the disturbance signals at the monitoring sensors, \mathbf{d} , via the matrices of transfer responses \mathbf{R} and \mathbf{P} respectively. The matrix of transfer responses from the secondary sources, \mathbf{u} , to the monitoring sensors, \mathbf{y} , is denoted \mathbf{G} , but it is assumed that any feedback from the secondary sources to the reference sensors, \mathbf{F} , is cancelled out by a perfect model, $\hat{\mathbf{F}}$ equal to \mathbf{F} , within the overall controller as explicitly shown in Fig. 1(b).

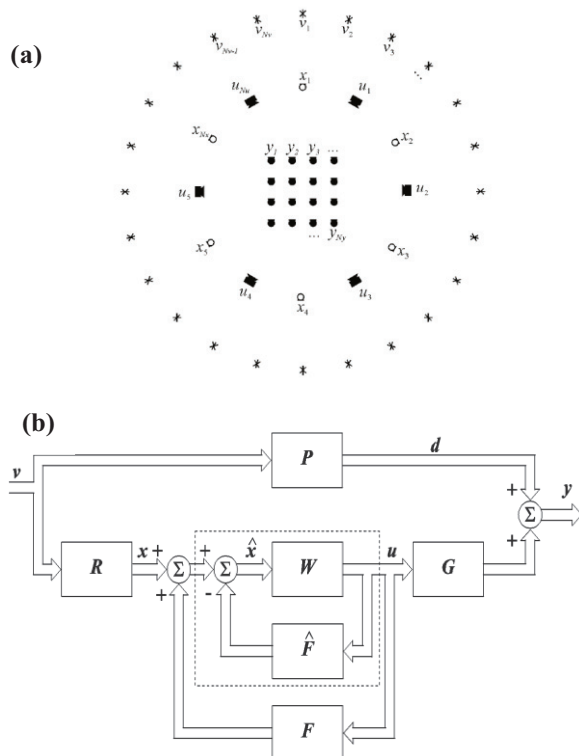


Fig. 1. (a) Geometric arrangement assumed for active control and (b) The block diagram of the feedforward active control system

The matrix of control filters, \mathbf{W} , which drive the secondary sources from the reference sensors, is thus entirely feedforward and the vector of signals at the monitoring sensors can be written as

$$\mathbf{y} = \mathbf{d} + \mathbf{G} \mathbf{W} \mathbf{x}. \quad (2)$$

The cost function to be minimised is a weighted sum of the modulus squared signal from the monitoring sensors, which can be written as

$$J = E[\mathbf{y}^H \mathbf{A} \mathbf{y}] = \text{trace} \mathbf{A} E[\mathbf{y} \mathbf{y}^H], \quad (3)$$

where \mathbf{A} is a square Hermitian ‘‘aperture’’ matrix, through which the error signals to be minimized are selected from all of the monitoring sensors. It is assumed in the simulations below, that \mathbf{A} is a real, diagonal, matrix, and is used to select the few monitoring signals to be minimised out of the whole array.

The second form of the cost function in equation (3) can be expanded out using equation (1) to give [5]

$$J = \text{trace} [\mathbf{A} \mathbf{G} \mathbf{W} \mathbf{S}_{xx} \mathbf{W}^H \mathbf{G}^H + \mathbf{A} \mathbf{G} \mathbf{W} \mathbf{S}_{xd}^H + \mathbf{S}_{xd} \mathbf{W}^H \mathbf{G}^H \mathbf{A}^H + \mathbf{S}_{dd}], \quad (4)$$

where the spectral density matrix for the reference signals, and the cross spectral density matrix between the output of the reference and detection sensors, are defined to be

$$\mathbf{S}_{xx} = E[\mathbf{x} \mathbf{x}^H], \text{ and} \quad (5)$$

$$\mathbf{S}_{xd} = E[\mathbf{d} \mathbf{x}^H]. \quad (6)$$

A generalisation of the result derived in [5] then allows the optimum set of control filters to be obtained that minimise the cost function in equation (4), as

$$\mathbf{W}_{opt} = -[\mathbf{G}^H \mathbf{A} \mathbf{G}]^{-1} \mathbf{G}^H \mathbf{A} \mathbf{S}_{xd} \mathbf{S}_{xx}^{-1}, \quad (7)$$

where it is assumed that both $\mathbf{G}^H \mathbf{A} \mathbf{G}$ and \mathbf{S}_{xx} are invertible. The influence of the spatial distribution of the primary field on the shape of the 10dB zone of quiet is illustrated in Fig. 2, for a local control system with a secondary source at $(L, 0)$ cancelling the sensor at $(0, 0)$, at a normalized excitation frequency of kL equal to 0.5, where k is the wave number. The shape of the zone of quiet for the simulations of the diffuse sound field, which was achieved with 408 uncorrelated sources as a sphere

in the far field, is the same as that in [9]. Also shown in this figure is the shape of this zone when only 21 uncorrelated primary sources are operating, either above or to the right or to the left of the quiet zone. The zone of quiet is greatest when the primary field is mainly from above, since in this case the primary pressure field is almost uniform in the plane shown in Fig. 2, so that reductions at the control point will result in similar reductions at all positions which are a similar distance from the secondary source. When the primary field is mainly from the right, the zone of quiet is somewhat broader in the x-direction than that achieved with a diffuse primary field, since the phase variation of the primary field then more nearly matches that of the secondary field in this direction. Conversely, when the primary field is mainly from the left, the phase variations of the primary and secondary field match more accurately in the y-direction, and so the extent of the quiet zone has instead been extended in this direction.

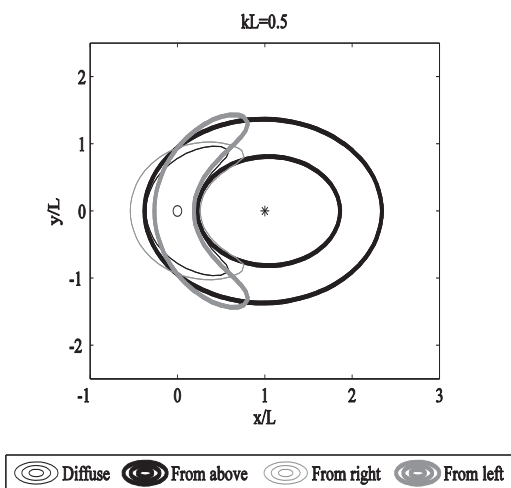


Fig. 2. The extent of the 10 dB zone of quiet, for a local control system of a normalized excitation frequency of $kL=0.5$, when the simulation field is diffuse, thin solid black line, mainly coming from above, thick solid black line, mainly from the right hand side, thin dash grey line, and mainly from the left hand side, thick solid grey line

3. Measurements in a stationary car

A series of measurements were made in a medium-size car, a Ford S-MAX, using an array of 25 microphones, as illustrated in Fig. 3, mounted on a 0.4 by 0.4 m grid positioned in front of the headrest on the front passenger seat. 12 of the microphones were in an upper grid and 13 in a lower grid, which

were separated by 75 mm. Two secondary loudspeakers were also mounted in the headrest and the frequency responses measured between the secondary sources and all of the microphones, giving the 25×2 matrix G in this case. The frequency response was also measured from a loudspeaker used to simulate the primary source to all the microphone locations. This loudspeaker was moved around to 96 positions on the front, sides, roof, floor and rear of the vehicle to measure the columns of the 25×96 element matrix P in this case, over a range of frequencies. In these initial simulations the reference microphones were assumed to be calculated with the monitoring microphones, so that the matrix R was equal to P in this case.

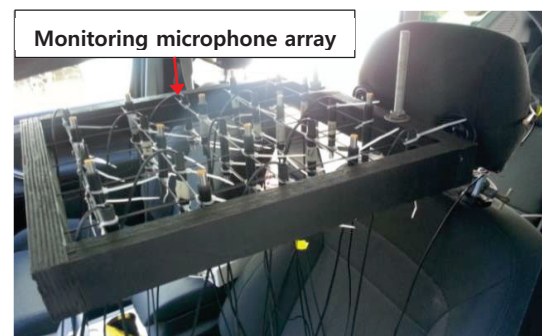
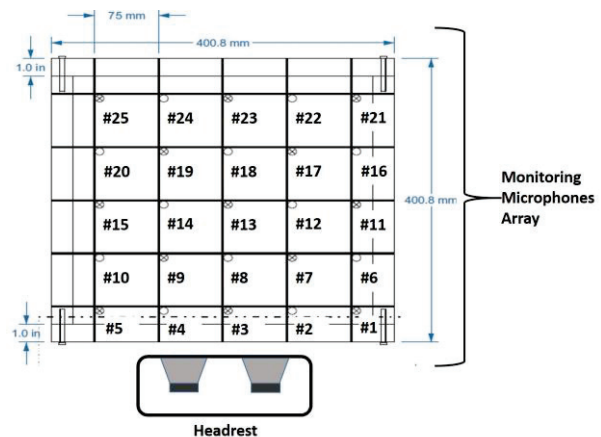


Fig. 3. The geometry of the microphone array and its installation on the front passenger seat

The formulation in section 2 can now be used to calculate the attenuation in the sum of squared pressures at the 25 monitoring microphones, when using the two headrest loudspeakers as secondary sources, with any combination of primary sources driven by a given spectral density matrix. Fig. 4 for example shows the attenuation results when a single primary source, located in either the front or the rear of the vehicle, is used and also when all 96 primary

sources are assumed to be driven with uncorrelated white noise signals, so that \mathbf{S}_{yy} is equal to the identity matrix. This indicates that greater attenuation is achieved with the primary source in the rear of the vehicle.

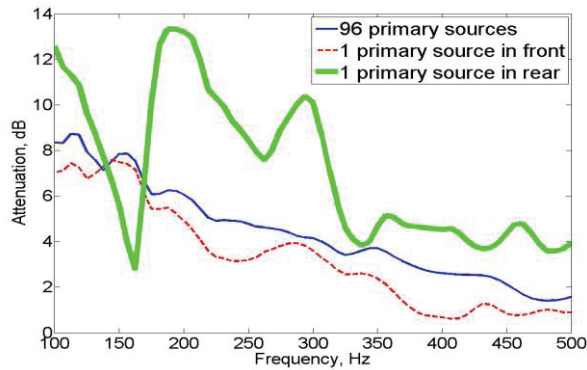


Fig. 4. Comparison of attenuations that are predicted in the sum of the squared pressures at all 25 monitoring microphones either with one primary in the front, or one primary in the rear or when all 96 primary sources are driven with uncorrelated white noise signals

The effect of the primary source location on the attenuation that can be achieved is also illustrated in Fig. 5, which shows the attenuation at all of the 25 microphone locations as a function of frequency when the primary source is assumed to be located in each of the 96 possible locations. It can be seen that, in general, better performance is obtained for primary sources placed above the microphone array or towards the rear of the vehicle, but there are considerable variations with primary source location and frequency.

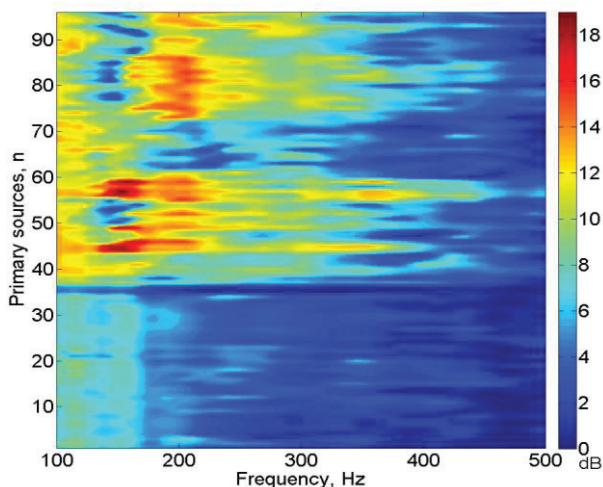


Fig. 5. A contour map of the attenuation at all 25 monitoring microphones using the two headrest secondary loudspeakers as a function of frequency and the location of a single primary source

Primary source position No.	Areas
1 ~ 5	Windshield
6~14	Dashboard
15~18	Front right floor
19~23	Front right door
24~28	Front left door
29~32	Front left floor
33~40	Front roof
41~49	Rear roof
50~55	Boot roof
56~61	Rear left door
62~67	Rear floor
68~72	Rear right door
73~80	Boot floor
81~86	Boot left wall
87~90	Boot right wall
91~96	Tailgate

Table 1. Primary source positions

4. Measurements in the car on the road

The vehicle was then taken on the road and driven at different speeds over different road surfaces. It was again assumed that perfectly correlated reference signals were available, by using the monitoring microphones as reference sensors, so the matrix $\mathbf{S}_{xd} \mathbf{S}_{xx}^{-1}$ in equation (7) just becomes the identity matrix and the spectral density after control becomes equal to

$$\mathbf{S}_{yy} = (\mathbf{I} + \mathbf{GW})\mathbf{S}_{dd}(\mathbf{I} + \mathbf{GW})^H \quad (8)$$

The power spectral density, PSD at each microphone before and after control is given by the diagonal elements of \mathbf{S}_{dd} and \mathbf{S}_{yy} . The sum of these PSDs are used as an overall measure of mean square pressure over the microphone grid, which are calculated from the trace of these matrices. Fig. 6 for example shows the A-weighted PSDs, averaged over all 25 microphones, when the car was driven at 50 mph on a relatively smooth road. Also shown in this figure is the predicted A-weighted average of the 25 PSDs when the two headrest loudspeakers are used to control the sound at four microphones in the second row in the array, calculated using the frequency domain theory in section 2. The A-weighted average of the PSDs at these four microphones only is also shown, before and after control. It can be seen that although reductions of about 20 dB are achieved at the four control microphones, up to frequencies of about 200

Hz, the average attenuation over the rest of the microphone array is only about 10 dB.

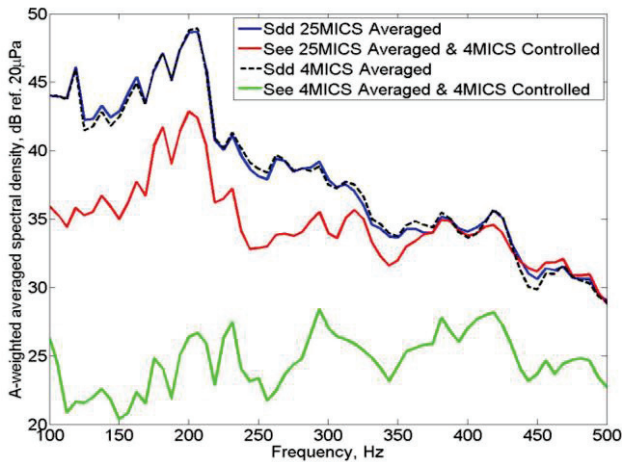


Fig. 6. A-weighted averaged PSD with/without two channel local active control systems which control 4 monitoring points with the physical microphone technique under the 50 mph driving

Fig. 7 shows the attenuation achieved for different frequencies at the 25 microphone positions, when these four microphones are controlled. Whereas a band of about 20 dB attenuation is achieved at the

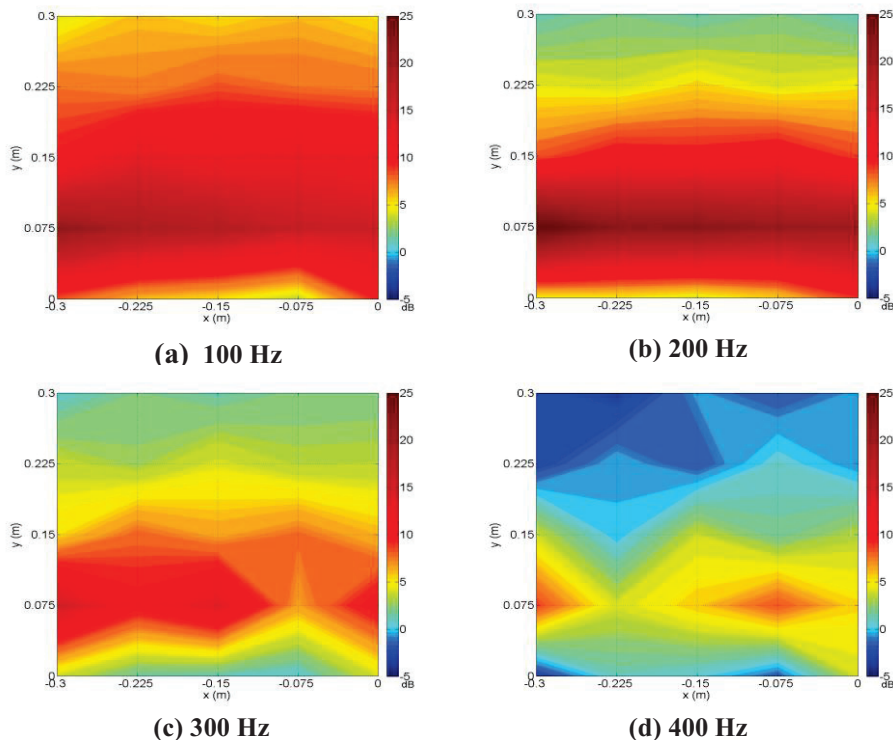


Fig. 7. Performance at all 25 microphones by the two channel local active control which controls the 4 selected microphone positions with the physical microphone sensing under the 50 mph driving : (a) 100 Hz (b) 200 Hz (c) 300 Hz (d) 400 Hz

control microphone locations up to 200 Hz, this becomes more local above this frequency.

The source of the primary sound field due to the road noise in the car can be estimated using the matrix of responses from the 96 loudspeaker locations on the boundaries of the vehicle to the 25 microphones, \mathbf{P} , and the inverse method of characterizing acoustic sound locations. Using the theory described in [10], the estimated spectral density matrix of the equivalent primary sources at 96 locations is given by

$$\tilde{\mathbf{S}}_{vv} = \{[\mathbf{P}^H \mathbf{P} + \boldsymbol{\beta} \mathbf{I}]^{-1} \mathbf{P}^H\} \mathbf{S}_{dd} \{[\mathbf{P}^H \mathbf{P} + \boldsymbol{\beta} \mathbf{I}]^{-1} \mathbf{P}^H\}^H, \quad (9)$$

where \mathbf{S}_{dd} is the spectral density matrix measured with the microphone array and $\boldsymbol{\beta}$ is a regularization factor chosen by trial and error to avoid ill-conditioning problems. The results are shown in Fig. 8, which indicates, for example, that at about 400 Hz, the road noise is mostly being produced by the dashboard, with some contribution from the left front door and left rear door.

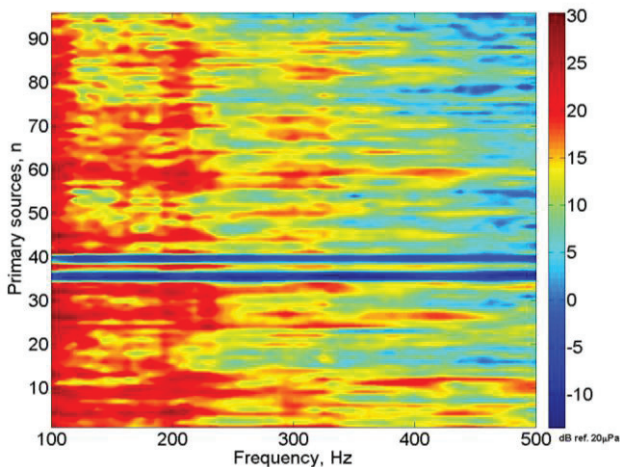


Fig. 8. The estimated contribution to the road noise in the test vehicle at 50 mph from the 96 assumed primary source locations, calculated using the inverse method from the measured signals at the 25 monitoring microphones in the array

5. Conclusions

A general formulation for calculating the optimal performance of local active sound control systems has been used to illustrate the effect of the spatial distribution of the primary field on the performance. In general, the performance of the controller is better for primary source locations above or behind the secondary source than it is in front, since in this case either the primary field is more uniform, or its phase more closely matches that of the secondary field. This is found both in free field simulations and in the simulations based on data measured in a car. The performance of a local system has also been investigated, controlling the road noise at 4 error microphones with 2 secondary loudspeakers mounted in the headrest. Good attenuations are predicted close to these microphones up to about 200 Hz. Finally, the source of the road noise within the vehicle has been estimated using an inverse method, using the transfer responses from 96 potential primary source locations in the vehicle to the 25 microphones.

The formulation presented here is in the frequency domain, for clarity, but time domain formulations, in which causality is imposed on the controller, are also possible [8]. Although some illustrative examples of results for particular control configurations have been presented here, it should be emphasized that the real power of the formulation is that it allows the performance of

many potential local control systems to be calculated off-line, given a set of simulated or measured data of the plant frequency responses and the spectral density properties of the reference and monitoring sensors. It is thus possible to rapidly investigate the effect of different reference signals and different secondary source and error sensor locations, for example, on the performance of local active control systems.

References

- [1] Thompson, D.J. and Dixon, J. (2004) Chapter 6: Vehicle noise. In, Fahy, F.J. and Walker, J.G. (eds.) *Advanced Applications in Acoustics, Noise and Vibration*. London, UK, Spon Press, 236-291.
- [2] Oh, S. H., Kim, H. S., & Park, Y. (2002). Active control of road booming noise in automotive interiors. *The Journal of the Acoustical Society of America*, 111(1), 180-188.
- [3] Sutton, T. J., Elliott, S. J., McDonald, A. M., & Saunders, T. J. (1994). Active control of road noise inside vehicles. *Noise Control Engineering Journal*, 42(4).
- [4] Elliott, S. (2000). *Signal processing for active control*. Academic press.
- [5] Rafaely, B., Elliott, S. J., & Garcia-Bonito, J. (1999). Broadband performance of an active headrest. *The Journal of the Acoustical Society of America*, 106(2), 787-793.
- [6] Pawelczyk, M. (2004). Adaptive noise control algorithms for active headrest system. *Control Engineering Practice*, 12(9), 1101-1112.
- [7] Garcia-Bonito, J., Elliott, S. J., & Boucher, C. C. (1997). Generation of zones of quiet using a virtual microphone arrangement. *The Journal of the Acoustical Society of America*, 101(6), 3498-3516.
- [8] Elliott, S. J., Cheer, J. (2015). Modelling local active sound control with remote sensors in spatially random pressure fields. *Submitted to The Journal of the Acoustical Society of America*.
- [9] Joseph, P., Elliott, S. J., & Nelson, P. A. (1994). Near field zones of quiet. *Journal of sound and vibration*, 172(5), 605-627.
- [10] Holland, K. R., & Nelson, P. A. (2013). The application of inverse methods to spatially-distributed acoustic sources. *Journal of Sound and Vibration*, 332(22), 5727-5747.